SOFT ROBOTICS Volume 11, Number 4, 2024 © Mary Ann Liebert, Inc. DOI: 10.1089/soro.2023.0076



Open camera or QR reader and scan code to access this article and other resources online.



ORIGINAL ARTICLE

# Worm-Inspired, Untethered, Soft Crawling Robots for Pipe Inspections

Yunwei Zhao, Haoran Huang, Weizhe Yuan, Xiaomin Liu, and C. Chase Cao<sup>2-4</sup>

#### **Abstract**

The increasing demand for inspection, upkeep, and repair of pipeline and tunnel infrastructures has catalyzed research into the creation of robots with superior flexibility, adaptability, and load-bearing capacities. This study introduces an autonomous soft robot designed for navigating both straight and curved pipelines of 90 mm diameter. The soft robot is enabled by an elongation pneumatic actuator (EPA) as its body and multiple radial expansion pneumatic actuators (REPAs) as its feet to provide adhesion and support on the pipe walls. It achieves a horizontal movement speed of 1.27 mm/s and ascends vertically at 0.39 mm/s. An integrated control mechanism, merging both pneumatic and electrical systems is employed to facilitate unrestrained movement. A novel control tactic has been formulated to ensure synchronized coordination between the robot's body deformation and leg anchoring, ensuring stable movement. This soft robot demonstrates remarkable mobility metrics, boasting an anchoring strength of over 100 N, a propelling force of 43.8 N when moving vertically, and a pulling strength of 31.4 N during navigation in curved pipelines. It can carry a camera to capture the internal view of the pipe and remove obstacles autonomously. The unconstrained and autonomous movement of the untethered soft robot presents new opportunities for various applications at different scales.

**Keywords:** soft robots, bioinspired robotics, worm-inspired robots, untethered robots, tubular robots, soft pneumatic actuators, modular design

# Introduction

 $\mathbf{T}$  he transportation of water, oils, and gases in industries often involves pipelines deployed in dangerous or inaccessible environments for humans. Thus, it is highly desirable to have an enabling robot to perform necessary inspection or repair tasks when necessary. However, designing robots that can navigate through these pipelines with stable and unconstrained movements has been a long-standing challenge in robotics.  $^{1-3}$ 

Presently, various mechanical designs such as wheeled, 4-7 tracked, 8-10 legged, 11,12 and snake-like 13-15 systems have been explored in the development of pipe robots. As Supplementary Table S1 highlights, many of these robots use rigid structural frameworks and typically rely on tethered, electrically powered systems. They are often most effective in larger pipelines, approximately greater than 100 A in diameter. Yet, a prevailing concern is that these conventional robots, tailored for infrastructure upkeep, predominantly comprise stiff materials and components. Such rigidity can impede their operation in

<sup>&</sup>lt;sup>1</sup>School of Mechanical Engineering, Beihua University, Jilin, China.

<sup>&</sup>lt;sup>2</sup>Department of Mechanical and Aerospace Engineering, Case Western Reserve University, Cleveland, Ohio, USA.

<sup>&</sup>lt;sup>3</sup>Department of Electrical, Computer, and Systems Engineering, Case Western Reserve University, Cleveland, Ohio, USA. <sup>4</sup>Advanced Platform Technology (APT) Center, Louis Stokes Cleveland VA Medical Center, Cleveland, Ohio, USA.

less predictable environments and can potentially pose safety risks. <sup>16–18</sup> For pipelines with diameters less than roughly 100 A, the application of these rigid robots becomes particularly arduous. The limited inner surface area complicates generating adequate propulsive force, thereby impeding the robot's ability to traverse extended distances or maneuver intricate routes. Considering these limitations, it is imperative to innovate soft robots. These robots, by virtue of their malleable design, can engage with their environment in a safer and more adaptive manner. This paves the way for broadening robotic applications, allowing them to better conform to varied environments and diverse mission specifications.

In light of these challenges, locomotion mechanisms resembling inchworm<sup>19–21</sup> or worm-like<sup>22–27</sup> movements emerge as particularly beneficial. Recently, the literature has seen a surge in the development of robots inspired by soft biological structures and crafted from malleable materials. These soft robots offer multiple advantages, such as enhanced flexibility, compliance, and a greater degree of freedom. This allows them to adeptly adapt and navigate through complex and unstructured terrains. 28-37 Researchers have explored the use of smart material-based actuators, such as shape memory alloys, 38 ionic polymer metal composites,<sup>39</sup> dielectric elastomer actuators (DEAs),<sup>40,41</sup> among others, to develop soft robots that generate deformation to move but have limited moving speed. More recently, soft robots driven by pneumatics, hydraulics, or vacuum have shown potential for pipeline applications. 42-46 However, most fluid-driven soft robots are tethered to external power supplies and control systems with cables, significantly restricting their functionality, particularly in applications such as search and rescue operations, undersea/space exploration, and environmental monitoring.<sup>17,47</sup> Furthermore, the inclusion of intricate and heavy cables can significantly augment the friction between the pipeline and the robot's appendages, complicating long-distance pipeline inspections. To circumvent the challenges posed by dragging extensive cables during these inspections, using batteries for untethered operations becomes essential. This approach substantially minimizes the robot's need for high traction, especially when considering constraints such as pipeline length, the number of bends, and the placement of corners. Consequently, robots can achieve greater agility and flexibility, making them better suited for extended, serpentine pipeline inspections.

In this work, we propose a new modular design for an untethered soft robot that can autonomously and stably crawl along a complex pipeline while carrying a payload, which is based on our previous tethered soft tubular robot.<sup>26</sup> The soft robot is composed of an elongation pneumatic actuator (EPA), which generates deformation in the soft robotic body, radial expansion pneumatic actuators (REPAs) that serve as feet to stick to the inner wall of the pipeline, and an independent control system that includes an electrical system and pneumatic system. All modules are connected in series by fast-inserting spherical joints, which provide high expansibility and flexibility, low cost, and ease of installation and maintenance. In addition, we developed a finite element model to aid in the design of the soft pneumatic actuators and conducted experiments to analyze their deformations and output force to predict the motion performance and load capacity of the soft robot. Our results demonstrate that the soft robot can carry a payload while crawling horizontally in a pipe and maintain stability when subjected to a resistance force of 43 N at the front of the robot or a backward pull exceeding 100 N at the end of the robot during one period of motion while crawling vertically. The specifically engineered soft actuators within the robot are adept at producing ample anchoring, propelling, and traction forces. These capabilities are sustained across horizontal and vertical orientations and are equally effective in both straight and curved pipes, ensuring that the crawling prerequisites for the 3.05 kg untethered robot are fully met.

The soft tubular robot is mechanically and electrically integrated and has a compact structure, high driving force, low cost, and ease of fabrication. Moreover, the untethered design enables it to navigate successfully through a complicated and unknown environment, providing more potential for its application.

#### **Results and Discussion**

For the intended application of inspecting PVC drainage pipes, which have an outer diameter of 90 mm and a wall thickness of 2 mm, featuring a flat and smooth interior, the robots are specifically designed to navigate long distances within pipes and negotiate the challenges posed by curves. We have opted for a worm-like locomotion method, recognizing its suitability for handling the twists and turns characteristic of complex pipeline systems, as well as its efficacy in performing inspections over extended stretches of pipe.

To align with the operational demands of the target pipeline, the design of the foot actuator is crucial; it must be able to generate an anchoring force robust enough to stabilize the robot's body against the inner pipe surface. Concurrently, the body actuator is tasked with producing sufficient actuation and traction forces to effectively propel the robot forward through the pipe, whether by pushing or pulling mechanisms. This dual requirement of anchoring and locomotion force generation is central to the robot's ability to perform its inspection tasks reliably and efficiently.

# Concept design and fabrication of the untethered soft crawling robot

As shown in Figure 1, we present a new modular design for an untethered soft robot that can autonomously crawl through complex pipelines like a worm. The control system and robot structure are integrated to enable autonomous motion. Our design is based on a previous, tethered soft tubular robot, with REPAs used as feet for adhesion to the inner surface of the pipeline, and an EPA used as the main body to propel the robot moving forward.

The design ingeniously houses the air source, power unit, and microcontroller within the space bridging the foot and body components, giving rise to an autonomous soft robot adept at navigating pipelines. In addition, a slender safety tether is affixed to the robot's rear, acting as a precautionary measure to avert the possibility of the robot becoming trapped within the pipe throughout the inspection process. The new prototype of the soft robot has a length of 1.2 m, a diameter of 8.2 cm, a mass of 3.05 kg, and can work for more than 2 h with a battery.

Dragon Skin30 was selected as the primary material for both the foot and body actuators due to its exceptional physical properties and flexibility. The actuators have a grid structure with

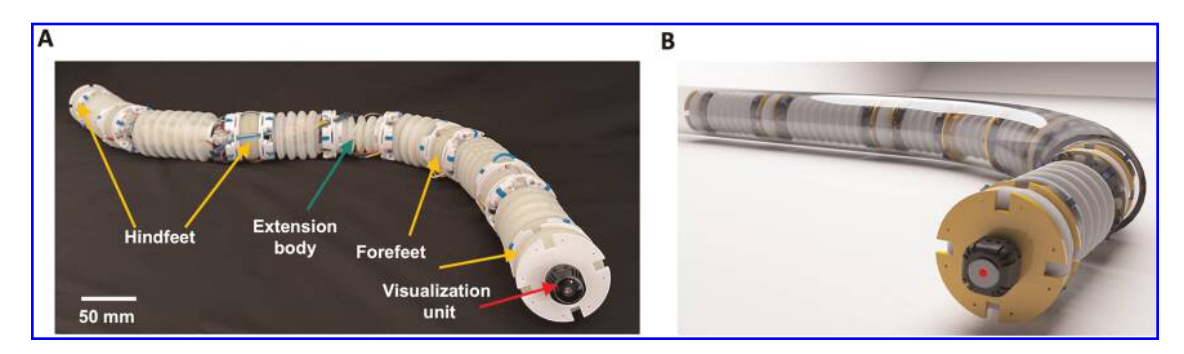


**FIG. 1.** The structure of the untethered soft pipe crawling robot. (A) The overall structural design of the robot. The robot is equipped with forefoot and hindfoot radial expansion pneumatic actuators (REPAs) that enable it to adhere to the inner surface of a pipeline, while the main body of the robot is propelled forward by the elongation pneumatic actuator (EPA). The air source, power, and microcontroller are integrated between the foot and foot or foot and body to form an untethered soft pipe crawling robot. The robot has the shape of a long worm with a visualization unit. (B) Demonstration of the untethered soft robot crawling in a pipe.

embedded pneumatic channels, as shown in Figure 2A. They are categorized into REPAs and EPAs based on their deformation under pneumatic pressure. REPAs expand radially and are cylindrical, making them ideal for supporting the robot's forefeet and hindfeet. EPAs, on the other hand, can elongate along the axial direction and act as the driving element for propelling the robot forward like a worm. The soft robot's

feet must carry the weight of the entire robot, including the gas pump, solenoid valves, relays, microcontroller, and battery, and a larger body than our prior tethered tubular robot. To address this, the radial size and wall thickness of REPAs were increased, while the inner chamber's volume was decreased (Supplementary Fig. S1 and Supplementary Table S1). This design allows for higher pressure with less gas volume, making it possible to

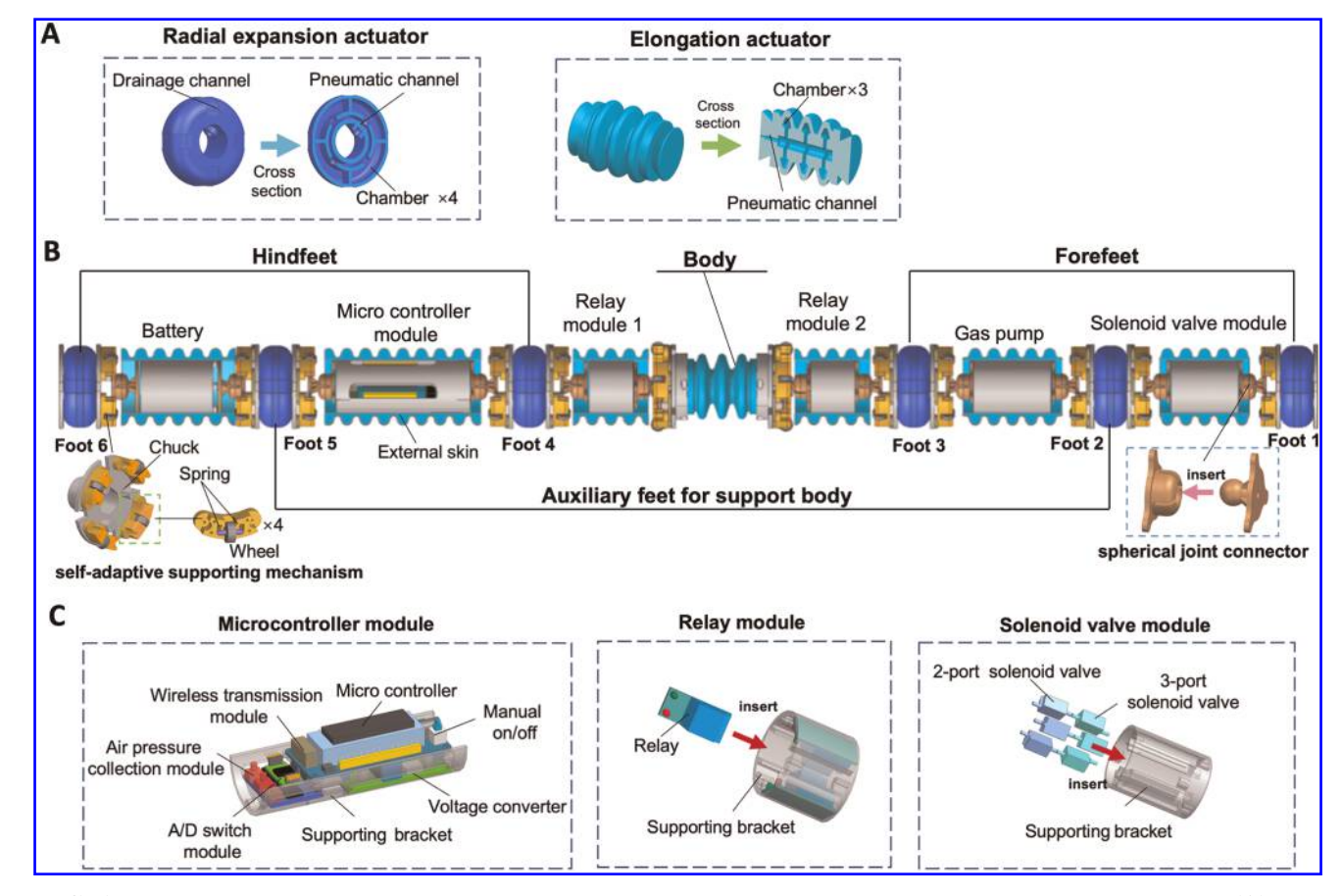


**FIG. 2.** The functional modules and internal construction design of the untethered soft pipe crawling robot. (A) The internal design of the pneumatic soft actuators, including the foot actuator and the body actuator. (B) The structure and position of each module of the soft robot, with the forefeet, body, and hindfeet connected in series by a spherical hinge. The electrical and pneumatic control system is arranged between the foot and the body. (C) The integrated design of the control system modules, packaged in custom-designed cylindrical supporting brackets.

carry the increased load while improving the robot's stability due to the higher anchoring force. The hollow structure of REPAs also facilitates positioning, installation, and connection.

To fabricate the REPAs and EPAs, the process involves mold casting of silicone elastomer (Supplementary Fig. S2). The first step is to design and assemble the molds for casting (Step I), followed by pouring the mixed silicone rubber (Dragon Skin 30, A: B = 1:1) into the mold for curing (Step II). The casted silicone rubber needs to be cured in an oven for 10 h before demolding. After demolding the cured components, the two parts of the actuator bond together with silicone rubber (Step III). We utilized a parametric modeling method for the mold, and the chamber mold was broken down into four parts and printed by a high-precision 3D printer, and then assembled. This provides a more accessible way to manufacture and assemble. The combination of parametric design and modular design is highly flexible and allows for simple and rapid modifications to the dimensions of REPA, which results in quick product customization.

#### Characterization of the REPAs and EPAs

REPA and EPA are essential components of the untethered soft pipe crawling robot, serving different functions. REPA supports the electrical and pneumatic systems while providing anchoring force and stability, while EPA drives the robot forward by propelling the control system. To ensure these actuators' mechanical performance, a Laser range finder (HG-C1200) and six-axis force sensor (SRI-V-171120-A M3703B SN2704) were used to measure their deformation and output force (Supplementary Fig. S3). The radial expansion of REPA increases with air pressure, reaching a maximum of 10 mm at 100 kPa; allowing the robot to adapt to different pipe diameters. The output force increases rapidly with air pressure, reaching 70 N at 100 kPa, ensuring stability. EPA elongates approximately linearly with air pressure, reaching a maximum of 80 mm at 100 kPa. The output force generated by EPA increases significantly with air pressure, reaching 120 N at 100 kPa. These tests confirm the actuators' driving and supporting abilities, ensuring the robot's effective performance. Images of the actuators' deformation under different air pressures are provided in Supplementary Fig. S4.

The experiments conducted on the load-carrying capability of the actuators in the pipeline and the anchoring force of REPA in different environmental conditions demonstrate the high performance and adaptability of the untethered soft pipe crawling robot. The EPA can lift a mass of 6.75 kg, representing a net payload capacity of 1.8 times the total mass of the robot. The REPA can hold a mass of 14 kg, which is 4.7 times the total mass of the robot, with an applied air pressure of 120 kPa (Supplementary Fig. S5A and Supplementary Videos S1). The radial output force of REPA increases rapidly to a steady state as soon as the air pressure is supplied, indicating the high performance of REPA under a certain range of diameters of the pipeline (Supplementary Fig. S5B and Supplementary Fig. S5C). In addition, REPA's anchoring capability was tested in dry, wet, fog, and oilcovered vertical pipes (Supplementary Fig. S5D and Supplementary Videos S2), and it was found that REPA remains stable in a dry pipe when the pulling force reaches 100 N. In an oil-covered pipe, the pulling force is reduced to 52 N due to slippage, while it tends to slide when the pulling force is 88 N and 82 N in wet and fog pipes, respectively. The high load-carrying capability and excellent anchoring force of REPA make the untethered soft pipe crawling robot adaptable to different environmental conditions, verifying its robust performance in a complicated environment.

# Assembly of the untethered soft robot

The current untethered soft robot is designed with a modular approach, consisting of a foot module, body module, and control system, which includes an electrical control system and a pneumatic control system. The electrical control system is composed of a microcontroller module, relay module, and battery, whereas the pneumatic control system is made up of a solenoid valve module and gas pump. To ensure proper mass distribution, each module of the control system is positioned between the foot and body or foot and foot. The heavier components, such as the gas pump and battery, are situated at the front and back of the body, respectively. The chucks on both sides of the foot actuator and body actuator can be screwed together with a screw thread. In addition, the chuck features four circumferential supporting wheels, with two springs each, creating a self-adaptive supporting mechanism that helps maintain the robot's position and posture. The supporting wheel's outer part that extends from the chuck can be adjusted passively to better adapt to the pipe diameter and minimize friction between the robot and the pipe wall. Furthermore, the modular design's spherical joint connection allows for increased flexibility and easy assembly and disassembly.

In this design, four of the robot's feet (foot 1, foot 3, foot 4, and foot 6) are inflated to perform the robot's main work, while foot 2 and foot 5 act as auxiliary feet to support the robot. However, they can also be used as backup foot actuators if necessary. To protect the control components, the modules of the control system are covered with soft skin made of Dragon Skin 30. The integrated design of the control system modules is shown in Figure 2C, where all the components are packaged within a cylindrical supporting bracket specifically designed for this purpose. These brackets are hollow cylindrical frameworks produced by a highprecision 3D printer, and they are used to accommodate the microcontroller module, solenoid valve module, and relay module. The interface of the supporting brackets is designed with grooves that match the dimensions of the components to achieve a better-integrated installation.

The microcontroller module comprises a microcontroller and other relevant electrical components, such as a manual on/off switch, voltage converter, A/D switch module, air pressure collection module, and wireless transmission module. These components are arranged strategically to make the module's structure compact and small. To reduce the module size and simplify the wiring process, only three relays (Risym 5V) are placed in a relay module, which is symmetrically distributed in the custom-designed supporting bracket. The solenoid valves are grouped into three categories, each consisting of a 2-port solenoid valve and a 3-port solenoid valve that control the inflation and deflation of the forefeet, hindfeet, and body actuator, respectively. By integrating the control system in custom-designed supporting brackets, the robot's configuration is compact and the size and mass of the robot are minimized.

# Control system and sensor integration

The control system for the untethered soft robot consists of an electrical system and a pneumatic system, as shown in Figure 3. The pneumatic system is responsible for supplying air to inflate and deflate the foot and body actuators, while the electrical system carries out long-range control commands from an upper computer to control the electrical components and solenoid valves of the pneumatic system to determine the inflation and deflation of the actuators. The electrical and pneumatic systems are coupled together and form a closed-loop control system for controlling the robot's motion. The electrical system comprises

a microcontroller module, two relay modules, and related electrical components. The microcontroller contains an Arduino bootloader for uploading, storing, and executing programs to control the soft robot. The air pressure collection module consists of sensors that measure the real-time air pressure of three gas circuits to actuate the forefoot, hindfoot, and body of the robot. The digital signal generated by the air pressure sensors is converted to analog through the A/D switch module and then transferred to the microcontroller to adjust the air pressure of the soft actuator. The relay modules are connected to the solenoid valves to control their on/off state to protect and switch the gas circuit of the actuators.

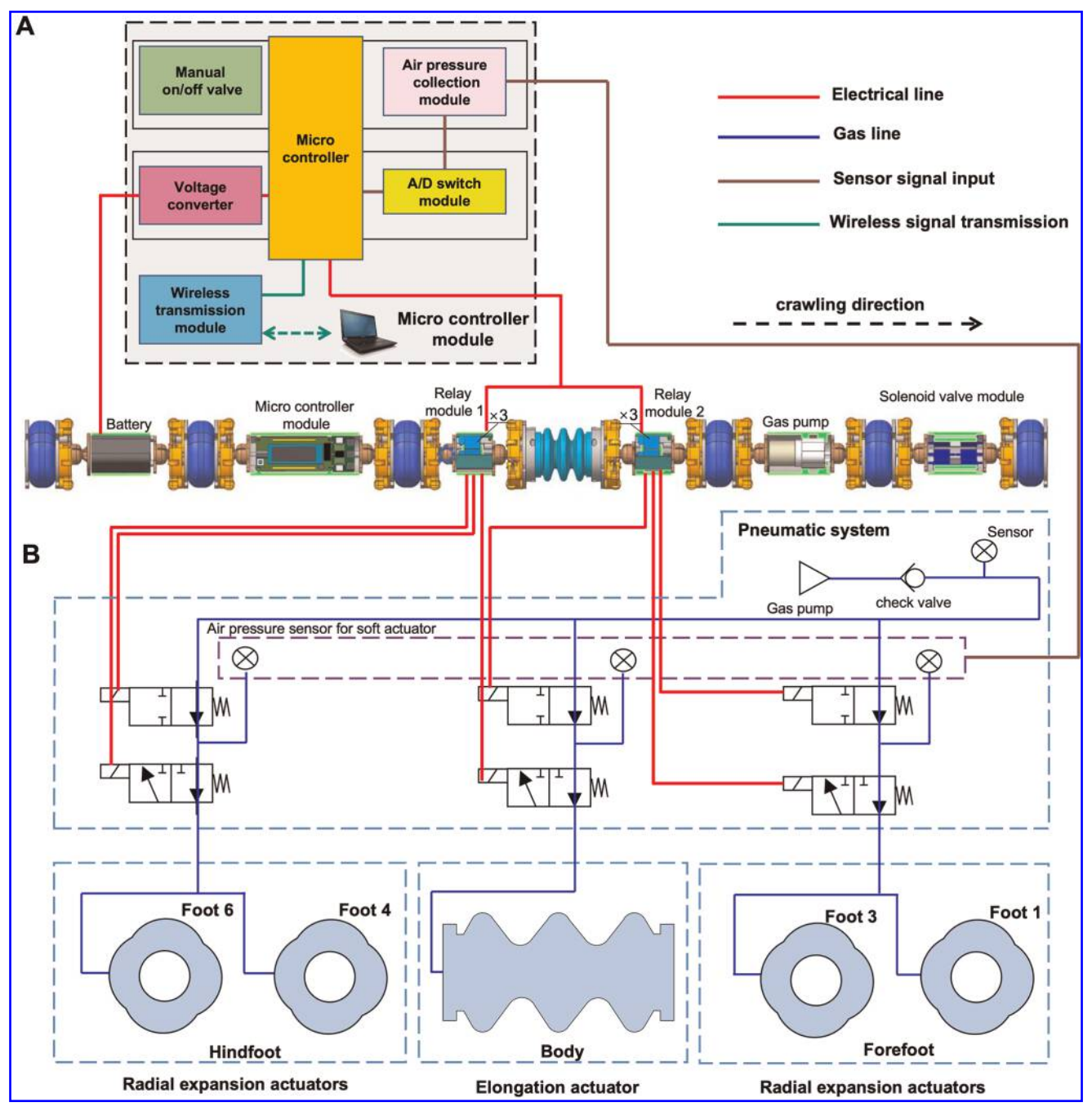


**FIG. 3.** The diagram of the control system. **(A)** The electrical system architecture of the soft robot shows the main control unit, motor drivers, wireless communication module, and power supply. **(B)** The pneumatic system schematic of the soft robot, including the air compressor, pressure regulator, solenoid valves, and pneumatic soft actuators.

The pneumatic system consists of a micro gas pump and a solenoid valve module. The micro gas pump provides a source of pressurized air at a constant rate, whereas the solenoid valve enables the changing-over connection of each actuator between this elevated pressure and atmospheric pressure. There are three sets of solenoid valves in series in the solenoid valve module, and each set valve comprises a 2-port solenoid valve and a 3-port solenoid valve. The three sets of solenoid valves, respectively, control five actuators of the soft robot, including two forefeet, two hindfeet, and one body actuator. The microcontroller analyzes the data and controls the on/off of the valves by the relay with the program. To actuate one of the actuators, the corresponding valve is opened to connect the actuator to the output of the micro gas pump. The extent of actuation of an actuator is controlled by the duration that the valve connecting to the micro gas pump was opened. The control programs, written and uploaded through the PL-2303SA interface, consist of a series of commands to control the control valves and micro gas pump and are stored in the onboard memory of the microcontroller. The robot can perform remote audio and visual observations by strapping a lightweight camera onto its body. The recorded video and audio files are transmitted to the upper computer through a wireless transmission module.

# Controls of single and cross gaits

We implemented a single gait that actuated the actuators of the soft robot in sequence from the hindfeet to the body and then to the forefeet, resulting in a peristaltic forward motion like a worm. As shown in Supplementary Fig. S6A, a single gait consists of a repeated sequence of six steps:

- Step 1: The hindfeet are pneumatically actuated to adhere to the inner wall of the pipe.
- Step 2: The body actuator of the soft robot inflates and axially elongates to push the forefeet to stride forward.
- Step 3: The forefeet are actuated to stick on the inner wall of the pipe.
- Step 4: The hindfeet are deflated to lift off from the inner wall of the pipe.
- Step 5: The body actuator deflates and pulls the hindfeet stride forward.
- Step 6: The hindfeet are actuated again to stick on the inner wall of the pipe.

Although the actuation of single gait resulted in forward motion at a velocity of 0.22 mm/s, there were still some unsatisfactory aspects of single gait crawling that need to be improved. Specifically, when the hindfeet are deflated in step 4, the robot's body is pulled down by gravity, resulting in a slide down of the hindfeet (Supplementary Fig. S6A–D). Similarly, in the first step of the next cycle, the body is compressed under the gravity of the forepart of the robot when the forefeet are deflated, causing another slide down of the soft robot (Supplementary Fig. S6A–G). This reveals the deficiency of single gait in a vertical pipe, as it is more suitable for heavy load operation in a horizontal pipe. To improve the applicability and practicability of the robot and avoid the downward slide of the robot in a nonhorizontal pipeline, we particularly studied the cross-gait mode, in

which the inflation or deflation of the feet actuator synchronizes with the elongation of the body actuator. Unlike the actuation in a sequence of single gait, the inflation and deflation of the body actuator in advance can pull or push the hindfeet or the forefeet in time, thus preventing the sliding phenomenon.

The cross-gait mode we studied consists of four steps, and the sequence diagram for each actuator is shown in Figure 4B. The internal air pressure characteristics of each actuator in a cycle are shown in Figure 4C, which were measured by the air pressure sensor (SMC PSE563). Figure 4A from b to e shows one cycle of the cross gait (Fig. 4A, a is the initial state):

- Step 1: The forefeet and hindfeet are both actuated to anchor to the inner wall of the pipe for a span of t<sub>f</sub>.
- Step 2: After t = t<sub>s</sub>, the body actuator is actuated in advance to push the forefeet to stride forward, while the forefeet actuators deflate to detach from the inner wall of the pipe.
- Step 3: The body actuator is actuated continuously and inflated in this step, while the forefeet actuators are inflated again to touch the inner wall of the pipe.
- Step 4: After a short time delay (t = t<sub>t</sub>), the hindfeet actuators are deflated to detach from the inner wall of the pipe, and the body actuator is deflated to pull the hindfeet stride forward.

By repeating this cycle, the robot moves forward in a horizontal pipeline. We also conducted experiments of robot crawling in a vertical pipe to demonstrate that cross gait significantly alleviates the sliding phenomenon (Supplementary Fig. S6B). The marker on the forefoot was tracked by a 3D motion capture system (NDI Optotrak) to quantitatively compare the displacement of the robot using single gait and cross gait. Supplementary Fig. S6 and Supplementary Videos S3 show the comparison of displacement of the robot using single gait and cross gait in a vertical pipe. The displacement of the robot using a single gait was lower compared with a cross gait due to slipping, and the maximum slippage was 2.9 mm. On the other hand, cross gait provides a more efficient way to control the robot, and its maximum slippage was only 0.9 mm in the ventilation process, much less compared with single gait.

# Kinematic analysis of the untethered soft robot

The kinematic performance of the untethered soft robot was evaluated using a 3D motion capture system, as shown in Figure 5A. The motion capture sensor (NDI Optotrak) was used to track the position of a marker on the gas pump and battery modules, located near the forefoot and hindfoot, respectively (Supplementary Fig. S7). The focus of the analysis was on the relationship between the moving speed of the robot under different air pressures and switching frequencies. Figure 5B displays photo images of the untethered soft robot crawling in a vertical pipe using the cross gait, with a period of 6 s. Real-time data were captured and analyzed digitally with the assistance of the 3D motion capture system (Supplementary Video S4), and the speed was calculated as 0.39 mm/s at a step frequency of 0.17 Hz.

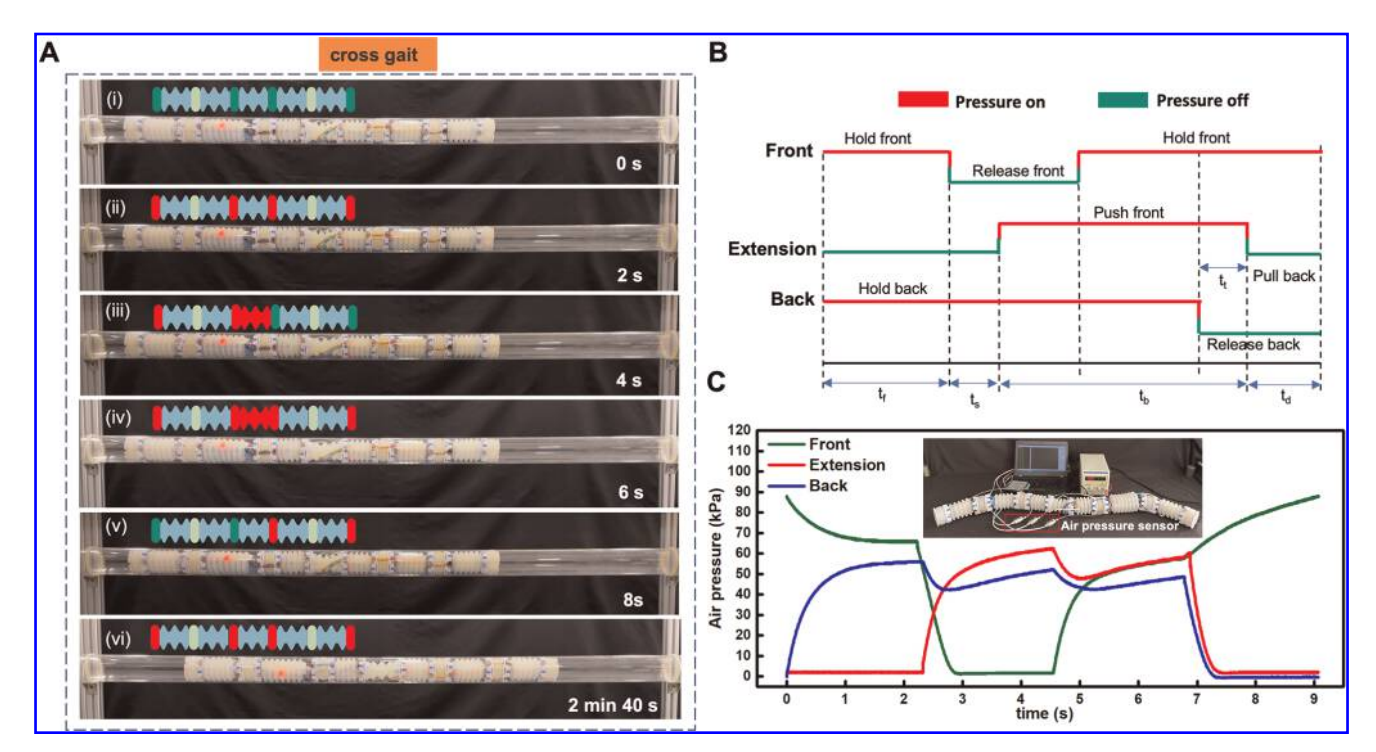


**FIG. 4.** Cross gait of the untethered soft robot. (**A**) Frames from movies of the robot performing cross gaits. The robot starts from the initial state (**a**), and both the forefeet and hindfeet are actuated to adhere to the inner wall of the pipe (**b**). The forefeet deflate, and then the body is actuated to push the forefeet forward (**c**). The forefeet are actuated again to touch the inner wall of the pipe (**d**). The hind feet deflate first, and then the body actuator deflates and pulls the hindfeet forward (**e**). This cycle repeats, and the robot moves forward in a horizontal pipeline at 1.27 mm/s (**f**). (**B**) A sequence diagram of the crossing gait. (**C**) The internal air pressure characteristic of each actuator in a complete cross-gait cycle.

Figure 5C and Supplementary Video S5 depict the soft robot's motion in a horizontal pipe using the cross gait with step frequencies of 0.5 Hz, 0.25 Hz, and 0.17 Hz, respectively. The displacement of the soft robot corresponding to each step frequency is illustrated in Figure 5D, based on the data collected by the 3D motion capture system. As time progressed, the displacement of the soft robot increased, with larger step frequencies resulting in greater displacement. The speed of the soft robot in the horizontal pipe was measured as 1.27 mm/s, 1.02 mm/s, and 0.73 mm/s when the step frequency was 0.5 Hz, 0.25 Hz, and 0.17 Hz, respectively.

# Performance evaluation and demonstration

The effectiveness of the untethered soft robot is verified through laboratory experiments, as shown in Supplementary Video S6. To facilitate remote audio and visual observations, a lightweight camera is mounted on the front end of the robot. Figure 6A illustrates the robot crawling in a pipe with obstacles inside, which in this case is a hollow sponge. During movement, the robot continuously captures the internal view of the pipe and follows the control system's instructions to proceed forward until obstacles are removed. Figure 6B and Supplementary Video S7 demonstrate the anchoring and driving forces of the robot in both horizontal and vertical pipes. The feet actuators are fixed at an air pressure of  $p_f = 90$  kPa, and the body actuator is set to  $p_b =$ 90 kPa. When attempting to pull the hindfoot backward, it is observed that the hindfeet remain adhered to the inner wall of the pipe even when the pulling force reaches 101.2 N in the horizontal pipe and 102.1 N in the vertical pipe (the pulling movement is completed in one period motion). Similarly,

when attempting to resist the forefoot, the maximum force measured by the dynamometer (SF-500) is 86 N in the horizontal pipe and 43.8 N in the vertical pipe due to the need to support the weight of about 4 kg.

Traction force is a key mechanical characteristic for evaluating the ability of worm-like locomotive soft robots to pull their posterior segments. Supplementary Fig. S8 and the Supplementary Video S8 showcase the body actuator's traction capabilities within both straight and curved pipelines. For this test, a dynamometer is connected to the robot's rear foot with a steel cable, which is then anchored to a fixed platform. To simulate the robot's traction movement, the rear foot is deflated to detach from the pipeline's inner wall, and the body actuator contracts to draw the rear foot forward. In straight pipes, the traction force registered by the dynamometer reaches 43.3 N. This force diminishes to 31.4 N in curved pipes, a reduction attributed to the body actuator's deformation as it conforms to the pipe's curvature. Notably, the minimum traction force recorded still surpasses the total weight of the robot's body. The robot's robust anchoring and propelling features significantly enhance its practicality and reliability for pipeline inspections.

The practicality and reliability of the robot are further demonstrated in the experiment of removing obstacles in the pipeline, as shown in Figure 6C and Supplementary Video S6. Iron bars weighing 5 kg are placed in the pipeline, a little distance from the robot, and it is observed that the robot continues to crawl forward after contact with the bars until it pushes them to the outlet of the pipeline. The motion performance of the soft robot carrying a heavy load is investigated using a 3D motion capture system. As shown in Figure 6D, the speed of the

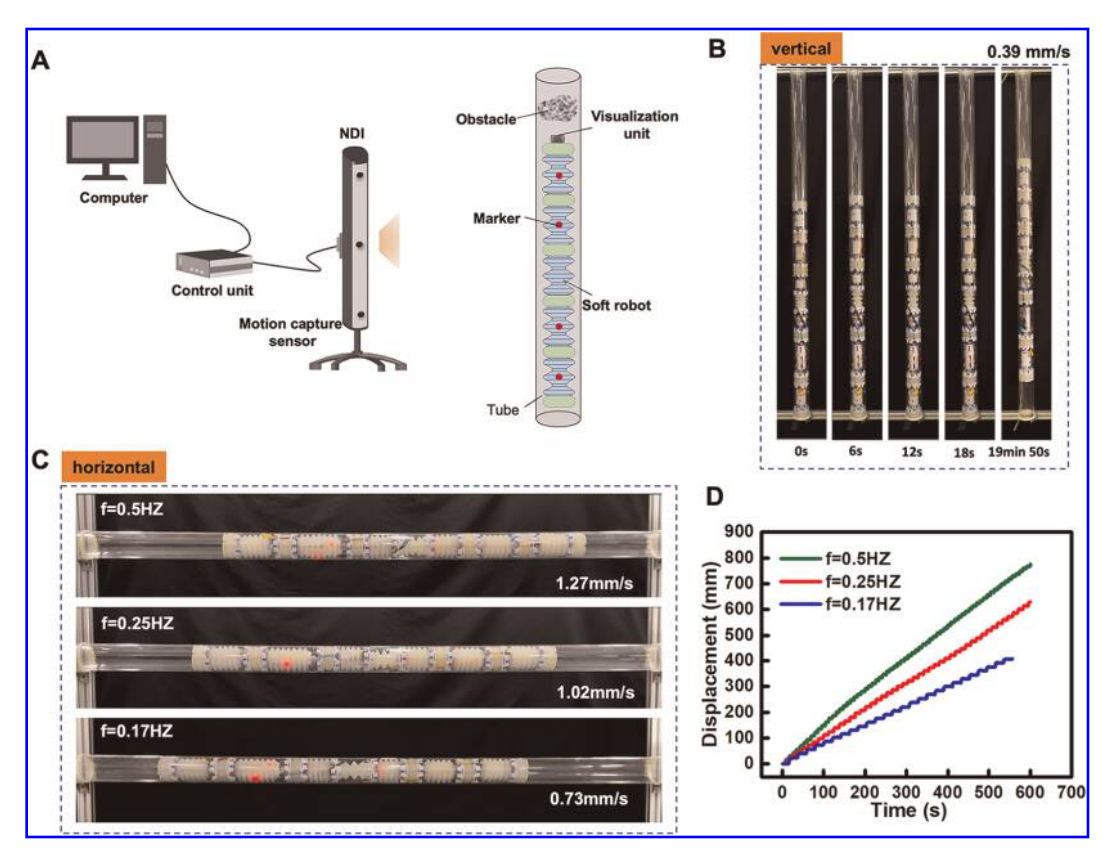


**FIG. 5.** Performance evaluation of the untethered soft robot in a pipe. (A) The principle for evaluating the motion performance of the untethered soft robot. (B) Photo images from experiments of the untethered soft robot crawling in a vertical pipe. (C) Photo images from experiments of the soft robot crawling with different step frequencies in a horizontal pipe. (D) The comparison of the displacement of the soft robot with different step frequencies in a horizontal pipe.

soft robot is 1.27 mm/s, which reduces to 0.74 mm/s (almost 41%) when the robot contacts an obstacle. Figure 6E shows the crawling speed of the robot in a horizontal pipe under different loads (error bars represent standard deviations). The robot's speed decreases with the increase in the mass of the obstacle due to growing friction. Supplementary Fig. S9 and Supplementary Video S9 illustrate the navigation capability of the soft robot in a curved pipe. As shown in Supplementary Fig. S9, the soft robot can stably crawl and successfully cross the 75° bend with a radius of 500 mm. It was demonstrated that the designed soft actuators are capable of expanding and contracting normally even in curved pipes, and that the soft robot can execute in the desired pipeline. The untethered design and robustness of the soft tubular robot make it suitable for various tasks, including inspection, obstacle removal, and maintenance.

# Conclusion and future work

In summary, we have successfully developed an untethered tubular soft robot that utilizes pneumatic soft actuators to achieve stable locomotion, building on a previous tethered soft robot design. Our modular design integrates all necessary components into appropriate modules, which are then connected in series using chucks and spherical joints. This approach not only makes the robot easy to assemble and disassemble but also enhances its robustness and flexibility. We have designed independent pneumatic and electrical systems for the robot, allowing wireless communication-based remote control and audiovisual data acquisition. By exploring the worm wriggle mechanism,

we investigated two gaits and demonstrated that our robot could achieve a speed of 1.27 mm/s in a horizontal pipe and 0.39 mm/s in a vertical pipe. In our experiments, we demonstrated the impressive mechanical performance of our soft actuators and soft robots. The foot actuator can hold a mass of 14 kg, and the body actuator can lift a mass of 6.75 kg in a vertical pipe. Remarkably, our robot can remain stable even when subjected to a backward pull that exceeds 100 N in one period of motion during crawling, due to its anchoring capability. The driving force of the soft robot reaches 43.8 N in a vertical pipe during crawling, which enhances its adaptability and functionality. The unconstrained movement of our soft robot makes it ideal for inspecting, cleaning, and maintaining pipelines and tunnels with convenience and maneuverability.

Our research will open avenues for significant advancements and practical applications. For instance, by refining the design and enhancing the integration of the electrical and pneumatic control systems, we could develop a smaller, elongated worm-like soft robot that moves at higher speeds. On the other hand, addressing the challenges identified will lead to a more functional robot. Enhancing the durability of the materials used for the soft actuators is critical, specifically improving their tear and wear resistance, to bolster the robot's resilience against corrosion and abrasion. As illustrated in Supplementary Fig. S10, our future efforts will focus on refining the design of the protective black rubber coating and its manufacturing process to achieve these improvements.

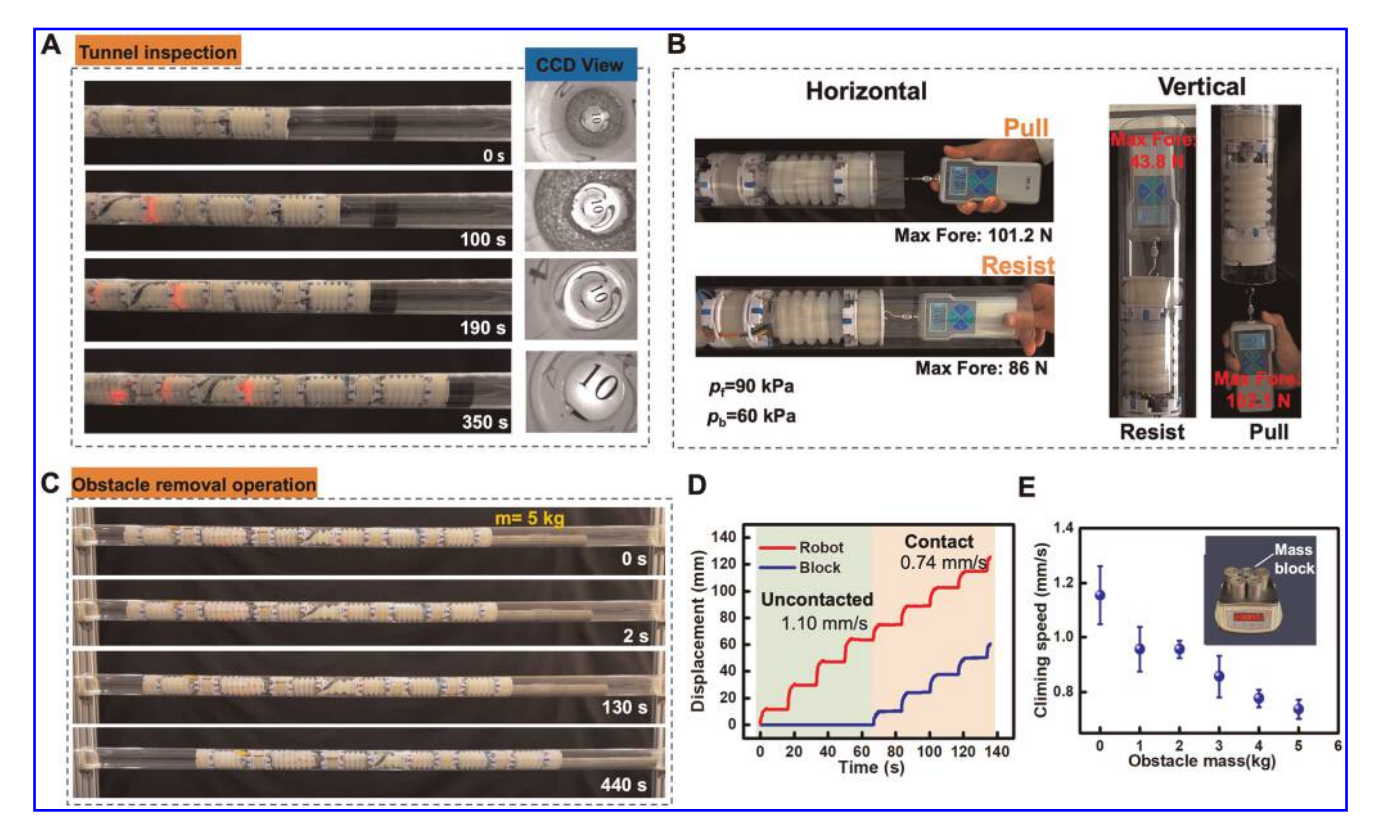


**FIG. 6.** Demonstration of application experiment of the untethered soft robot. (A) The soft robot executes inspection and obstacle removal. The soft robot is shown exploring the inside of a pipe, as well as removing obstacles along the way. (B) Evaluation of anchoring force and driving force of the soft robot in the process of crawling. The graph shows the force measurements during the crawling process, including the maximum force that can be sustained without losing stability. (C) The soft robot removes a much heavier block in the pipe. The mass of the heavy block reaches 5 kg. (D) Comparison of motion performance before and after contact with obstacles. The graph shows the difference in speed and stability of the robot before and after it encounters an obstacle. (E) The crawling speed of the robot in a horizontal pipe under different load conditions. Error bars represent standard deviations. The graph shows the relationship between the load carried by the robot and its crawling speed.

# **Authors' Contributions**

Y.Z., X.L., and C.C. conceptualized and designed research; Y.Z., H.H., M.S. conducted the experiments; all authors interpreted and analyzed the data; Y.Z., X.L., and C.C. drafted and edited the article; all authors provided comments and revision of the article.

# **Author Disclosure Statement**

No competing financial interests exist.

# **Funding Information**

Y.Z. and X.L. acknowledge the financial support from the Department of Science and Technology of Jilin Province, China (YDZJ202201ZYTS624) and (YDZJ202401396ZYTS), Graduate School of Beihua University (JG2021038), and Science and Technology Bureau of Jilin (JJKH20156413). C.C. acknowledges the financial support from US NSF (ECCS-2024649) and Case Western Reserve University.

# **Supplementary Material**

Supplementary Figure S1 Supplementary Figure S2 Supplementary Figure S3 Supplementary Figure S5 Supplementary Figure S6 Supplementary Figure S7 Supplementary Figure S8 Supplementary Figure S9 Supplementary Figure S10 Supplementary Table S1 Supplementary Table S2 Supplementary Video S1 Supplementary Video S2 Supplementary Video S3 Supplementary Video S4 Supplementary Video S5 Supplementary Video S6 Supplementary Video S7 Supplementary Video S8 Supplementary Video S9

Supplementary Figure S4

# References

- 1. Rus D, Tolley MT. Design, fabrication and control of soft robots. Nature 2015;521(7553):467–475; doi: 10.1038/nature14543
- Nansai S, Mohan R. A survey of wall climbing robots: Recent advances and challenges. Robotics 2016;5(3):14; doi: 10.3390/ robotics5030014

 Drotman D, Jadhav S, Karimi M, et al. editors. 3D printed soft actuators for a legged robot capable of navigating unstructured terrain. IEEE International Conference on Robotics & Automation; 2017.

- Roh SG, Choi HR. Differential-drive in-pipe robot for moving inside urban gas pipelines. IEEE Transactions on Robotics 2005;21(1):1–17.
- Roh S-G, Kim DW, Lee J-S, et al. In-pipe robot based on selective drive mechanism. Int J Control Autom Syst 2009; 7(1):105–112; doi: 10.1007/s12555-009-0113-z
- 6. Kwon YS, Lee B, Whang IC, et al. editors. A flat pipeline inspection robot with two wheel chains. IEEE International Conference on Robotics & Automation; 2011.
- Kakogawa A, Ma S, editors. Design of a multilink-articulated wheeled inspection robot for winding pipelines: AIRo-II. 2016 IEEE/RSJ International Conference on Intelligent Robots and Systems (IROS); 2016.
- Kim JH, Sharma G, Iyengar SS, editors. FAMPER: A fully autonomous mobile robot for pipeline exploration. IEEE International Conference on Industrial Technology; 2010.
- Kwon Y-S, Yi B-J. Design and motion planning of a two-module collaborative indoor pipeline inspection robot. IEEE Trans Robot 2012;28(3):681–696; doi: 10.1109/tro.2012.2183049
- Kakogawa A, Ma S. Effect of underactuated parallelogram shape-shifting for environmental adaptation movement of a three modular in-pipe robot. Front Robot AI 2023;10: 1234835; doi: 10.3389/frobt.2023.1234835
- Lu Yi, Yu Jingjing, Sui Chunping, et al. editors. Design of in-pipe 3SPR/3RPS parallel manipulator and its kinestatics analysis. 2015 IEEE International Conference on CYBER Technology in Automation, Control, and Intelligent Systems (CYBER); 2015.
- Savin S, Vorochaeva L, editors. Nested quadratic programmingbased controller for in-pipe robots. Proceedings of International conference on industrial engineering 2017; 2017.
- 13. Fjerdingen SA, Liljebäck P, Transeth AA, editors. A snakelike robot for internal inspection of complex pipe structures (PIKo). IEEE/RSJ International Conference on Intelligent Robots & Systems; 2009.
- 14. Schempf H, Mutschler E, Gavaert A, et al. Visual and non-destructive evaluation inspection of live gas mains using the Explorer™ family of pipe robots. Journal of Field Robotics 2010;27(3):217–249; doi: 10.1002/rob.20330
- 15. Kim HM, Choi YS, Mun HM, et al. editors. Design of back-drivable joint mechanism for in-pipe robot. IEEE/RSJ International Conference on Intelligent Robots and Systems (IROS), 2015; 2015.
- 16. Chattopadhyay P, Ghoshal S, Majumder A, et al. Locomotion methods of pipe climbing robots: A review. JESTR 2018;11(4):154–165; doi: 10.25103/jestr.114.20
- 17. Gu G, Zou J, Zhao R, et al. Soft wall-climbing robots. Sci Robot 2018;3(25); doi: 10.1126/scirobotics.aat2874
- 18. Waleed D, Mustafa SH, Mukhopadhyay S, et al. An in-pipe leak detection robot with a neural-network-based leak verification system. IEEE Sensors J 2019;19(3):1153–1165; doi: 10.1109/jsen.2018.2879248
- 19. Fang D, Shang J, Luo Z, et al. Development of a novel self-locking mechanism for continuous propulsion inchworm inpipe robot. Advances in Mechanical Engineering 2018;10(1): 168781401774940.

20. Xie Q, Liu S, Ma X. Design of a novel inchworm in-pipe robot based on cam-linkage mechanism. Advances in Mechanical Engineering 2021;13(9):168781402110451.

- Li M, Wang G, Wang J, et al. Development of an inchwormlike soft pipe robot for detection. International Journal of Mechanical Sciences 2023;253:108392; doi: 10.1016/j.ijmecsci .2023.108392
- Ishikawa R, Tomita T, Yamada Y, et al. editors. Development of a peristaltic crawling robot for long-distance complex line sewer pipe inspections. 2016 IEEE International Conference on Advanced Intelligent Mechatronics (AIM); 2016.
- Mano Y, Ishikawa R, Yamada Y, et al. editors. Development of contraction force control system of peristaltic crawling robot for sewer pipe inspection. 2018 IEEE/ASME International Conference on Advanced Intelligent Mechatronics (AIM); 2018.
- Zhang B, Fan Y, Yang P, et al. Worm-like soft robot for complicated tubular environments. Soft Robot 2019;6(3): 399–413; doi: 10.1089/soro.2018.0088
- Verma MS, Ainla A, Yang D, et al. A soft tube-climbing robot. Soft Robot 2018;5(2):133–137; doi: 10.1089/soro .2016.0078
- Liu X, Song M, Fang Y, et al. Worm-inspired soft robots enable adaptable pipeline and tunnel inspection. Advanced Intelligent Systems 2022;4(1):2100128.
- Tang C, Du B, Jiang S, et al. A pipeline inspection robot for navigating tubular environments in the sub-centimeter scale. Sci Robot 2022;7(66):eabm8597.
- 28. Yamamoto T, Sakama S, Kamimura A. Pneumatic duplex-chambered inchworm mechanism for narrow pipes driven by only two air supply lines. IEEE Robot Autom Lett 2020; 5(4):5034–5042; doi: 10.1109/lra.2020.3003859
- 29. Xie D, Liu J, Kang R, et al. Fully 3d-printed modular pipe-climbing robot. IEEE Robot Autom Lett 2021;6(2):462–469; doi: 10.1109/lra.2020.3047795
- Wehner M, Truby RL, Fitzgerald DJ, et al. An integrated design and fabrication strategy for entirely soft, autonomous robots. Nature 2016;536(7617):451–455; doi: 10.1038/nature19100
- Wang T. Soft Robotics:Structure, Actuation, Sensing and Control. JME 2017;53(13):1; doi: 10.3901/jme.2017.13.001
- 32. Wallin TJ, Pikul J, Shepherd RF. 3D printing of soft robotic systems. Nat Rev Mater 2018;3(6):84–100; doi: 10.1038/s41578-018-0002-2
- 33. Walker J, Zidek T, Harbel C, et al. Soft robotics: A review of recent developments of pneumatic soft actuators. Actuators 2020;9(1):3; doi: 10.3390/act9010003
- Gorissen B, Reynaerts D, Konishi S, et al. Elastic inflatable actuators for soft robotic applications. Adv Mater 2017; 29(43); doi: 10.1002/adma.201604977
- 35. Zhao W, Zhang Y, Wang N. Soft robotics: Research, challenges, and prospects. JRM 2021;33(1):45–68; doi: 10.20965/jrm.2021.p0045
- 36. Yuan P, Kawano G, Tsukagoshi H, Design and modeling of soft pneumatic helical actuator with high contraction ratio. JRM 2020;32(5):1061–1070; doi: 10.20965/jrm.2020.p1061
- Won P, Kim KK, Kim H, et al. Transparent soft actuators/sensors and camouflage skins for imperceptible soft robotics. Adv Mater 2021;33(19):e2002397; doi: 10.1002/adma.202002397
- 38. Seok S, Onal CD, Cho K-J, et al. Meshworm: A peristaltic soft robot with antagonistic nickel titanium coil actuators. IEEE/ASME Trans Mechatron 2013;18(5):1485–1497; doi: 10.1109/tmech.2012.2204070

- 39. Must I, Kaasik F, Põldsalu I, et al. Ionic and capacitive artificial muscle for biomimetic soft robotics. Adv Eng Mater 2015;17(1):84–94; doi: 10.1002/adem.201400246
- Cao J, Qin L, Liu J, et al. Untethered soft robot capable of stable locomotion using soft electrostatic actuators. Extreme Mechanics Letters 2018;21:9–16; doi: 10.1016/j.eml.2018 .02.004
- Pfeil S, Henke M, Katzer K, et al. A worm-like biomimetic crawling robot based on cylindrical dielectric elastomer actuators. Front Robot AI 2020;7:9; doi: 10.3389/frobt.2020 00009
- 42. Wang T, Ge L, Gu G. Programmable design of soft pneunet actuators with oblique chambers can generate coupled bending and twisting motions. Sensors and Actuators A: Physical 2018;271:131–138; doi: 10.1016/j.sna.2018.01.018
- 43. Wang X, Mitchell SK, Rumley EH, et al. High-strain peano-HASEL actuators. Adv Funct Materials 2019;30(7); doi: 10.1002/adfm.201908821
- 44. Qin L, Liang X, Huang H, et al. A versatile soft crawling robot with rapid locomotion. Soft Robot 2019;6(4):455–467; doi: 10.1089/soro.2018.0124
- 45. Tawk C, Spinks GM, In Het Panhuis M, et al. 3D printable linear soft vacuum actuators: Their modeling, performance quantification and application in soft robotic systems. IEEE/ASME Trans Mechatron 2019;24(5):2118–2129; doi: 10.1109/tmech.2019.2933027

- 46. Liu X, Zhao Y, Geng D, et al. Soft humanoid hands with large grasping force enabled by flexible hybrid pneumatic actuators. Soft Robot 2020;8(2):175–185.
- 47. Marchese AD, Katzschmann RK, Rus D. A recipe for soft fluidic elastomer robots. Soft Robot 2015;2(1):7–25; doi: 10.1089/soro.2014.0022

Address correspondence to:
X. Liu
School of Mechanical Engineering
Beihua University
Jilin
Jilin 132013
China

*E-mail:* xiaomin\_liu@beihua.edu.cn

C. Cao
Department of Mechanical and Aerospace Engineering
Case Western Reserve University
Cleveland
OH 44106
USA

E-mail: ccao@case.edu